Raman and Fourier transform infrared spectroscopic investigation of the effects of Er^{3+} doping in barium titanate ceramics

Z. Ž. LAZAREVIĆ[1,*], A. MILUTINOVIĆ[1], M. ĆURČIĆ[1], I. STAJČIĆ[2], B. HADŽIĆ[1], U. RALEVIĆ[1], V. PAUNOVIĆ[3]
[1]*Institute of Physics Belgrade, University of Belgrade, 11080, Belgrade, Serbia*
[2]*Department of Physical Chemistry, "Vinča" Institute of Nuclear Sciences—National Institute of the Republic of Serbia, University of Belgrade, Mike Petrovića Alasa 12-14, P.O. Box 522, 11351, Vinca, Belgrade, Serbia*
[3]*University of Niš, Faculty of Electronic Engineering, Aleksandra Medvedeva 14, Niš, Serbia*

In this work, we study the barium titanate doped different content Er^{3+} perovskite ceramics prepared by conventional solid-state sintering procedure. The as-made powder samples were pressed into a pellet shape and subsequently sintered at 1350 °C for 4 h in air. The structural, morphological, and optical properties of the synthesized samples were investigated by X-ray diffraction (XRD), scanning electron microscopy (SEM), atomic force microcopy (AFM), Raman and Fourier transform infrared spectroscopy (FTIR) spectroscopy, respectively. The XRD study revealed the formations of single phase tetragonal structure of barium titanate ($BaTiO_3$). The SEM analysis shows that all of measured samples are characterized by polygonal grains. The uniform and homogeneous microstructure with grain sizes from 20 to 45 μm is the main characteristic of the low doped samples (0.01 and 0.1 wt.% Er^{3+}). For the samples doped with the higher dopant concentration (0.5 and 1.0 wt.%) the average grains sizes have been ranged from 2 to 15 μm. Substitution of Er dopant into Ba-site reduced the grain sizes and roughness parameter of the $BaTiO_3$ which was attributed to the smaller ionic radius of Er. The Raman and the FIR reflective spectra measured in this work were fitted. The intensity of the Raman and IR bands of Er^{3+} doped barium titanate is higher than that of undoped BT that could suggest a structure change from tetragonal to pseudo-cubic. FTIR shifts confirmed the incorporation of Er^{3+} in $BaTiO_3$ at 1350 °C.

(Received June 15, 2024; accepted December 2, 2024)

Keywords: Er^{3+}, $BaTiO_3$, Raman spectroscopy

1. Introduction

Perovskites as barium titanate ($BaTiO_3$), with an ABO_3 general formula, have been extensively studied [1]. Structurally, perovskites form a crystal lattice based on oxygen or other anions in an octahedral arrangement, which generate two types of cavities: one with octahedral symmetry to accommodate small cations, generally tetra or pentavalent, and the other with dodecahedral symmetry, where cations of varying sizes, usually mono or divalent, can be hosted (Fig. 1). According to this, different cations may be accommodated in the crystalline lattice, either at the octahedral or dodecahedral site, depending on charge and ionic radius. These inserted ions create distortions of the original lattice which modify the material properties.

Modified $BaTiO_3$ ceramics is one of the most investigated dielectric materials due to its practical applications. The significance of this material is mainly based on its wide variety of applications such as multilayer ceramic capacitors (MLCCs), PTC thermistors, varistors, piezoelectric sensors, ultrasonic transducers, radio and communication filters and optoelectronic elements [2-4]. In particular, erbium-doped waveguides films have attracted much attention because of their use as optical amplifiers, which have been used in the detection of infrared radiation by converting the invisible light into the visible range where conventional detectors are effective also in optical storage, printing, display technology and medicine using up-conversion emission at 550 nm [5, 6]. Furthermore, $BaTiO_3$ is a very useful host matrix for some applications because it does not absorb energy, allowing it to serve only for support of rare earth ions, which is very useful for these particular applications [7-9]. In particular, rare earth (RE) doped NIR-to-visible ceramic oxides represent an alternative and excellent substitute for traditional fluorescent applications [10].

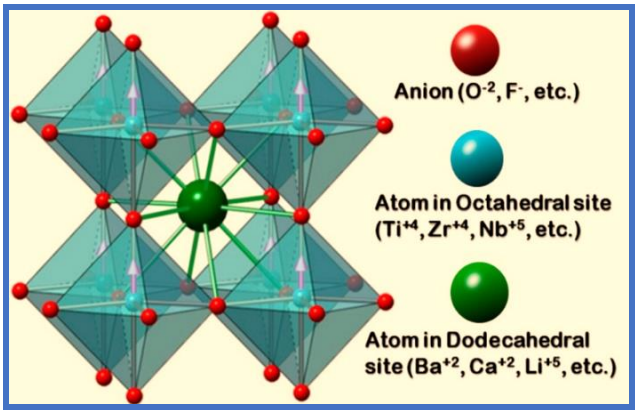

Fig. 1. Typical scheme for a perovskite lattice structure (color online)

The properties of the modified $BaTiO_3$ ceramics depend on the ceramics composition, synthesis method of starting powders, sintering procedure and obtained microstructure. The $BaTiO_3$ powder is usually mixed with additives in order to adjust the sintering parameters and electrical properties to the requirements of electronic device [11-12]. It is known that the electric properties, especially PTC effect of polycrystalline $BaTiO_3$, depend to a great extent on the grain growth during sintering as well as the type and concentration of donors or acceptor dopants [13-15]. In addition, the properties strongly depend on the site preference of dopant ions in $BaTiO_3$ sublattices. Two types of dopants can be introduced into $BaTiO_3$ lattice. Ions with larger ionic radius and low valence like Er^{3+}, Ho^{3+}, and La^{3+}, tend to enter the Ba^{2+} sites in perovskite lattice, while ions with smaller ionic radius and higher valence like Nb^{5+}, can be incorporated into the Ti^{4+} sublattice [16-25].

At low concentrations of Er^{3+} (below 0.5 wt.%), substitution of Ba^{2+} ions and formation of solid solutions occur. At higher concentrations of additives, over 0.5 wt.%, either Ba^{2+} or Ti^{4+} ions are substituted, causing very high electrical resistivity of the sample (ρ=108 Ωm). The substitution of Er^{3+} on Ba^{2+} sites require formation of negatively charged defects. For the samples sintered at air atmosphere, the principal doping mechanism is the ionic compensation mechanism (vacancy compensation mechanism) [26, 27]. The purpose of this paper is to analyze $BaTiO_3$ doped with various content of Er_2O_3, sintered at 1350 °C temperature. The influence of dopant on the microstructure and spectroscopy properties has been investigated.

The aim of this work is to prepare and investigate $BaTiO_3$ doped Er^{3+} and characterize their microstructural and spectroscopic properties.

2. Methods and materials

The samples $BaTiO_3$ doped of were prepared by conventional solid-state sintering procedure starting from high purity commercial $BaTiO_3$ powder (MURATA) with Ba and Ti ratio, [Ba]/[Ti]=1.005, and reagent grade Er_2O_3 powder (Fluka chemika). The content of additive oxides, Er_2O_3, is ranged from 0.01 to 1.0 wt,%.

Starting powders were ball-milled. After that were dried, and pressed under a uniaxial pressure of 120MPa into disks of 7 mm in diameter and 3 mm in thickness. The compacts are sintered at 1350 ºC in the air atmosphere for 4 hours.

X-ray diffraction (XRD) patterns are recorded with CuKα radiation in a PhilipsX'Pert diffractometer (Philips, the Netherlands).

The samples were etched in 10% HCl with 5% HF for the microstructure examination. The microstructures of as sintered or chemically etched samples were observed by scanning electron microscope (JEOL-JSM 5300) equipped with energy dispersive spectrometer (EDS-QX 2000S system). The grain size and porosity distribution of samples were obtained by LEICA Q500MC Image Processing and Analysis System.

The AFM measurements were conducted using the NTEGRA Prima system from NT-MDT. Topographical images were obtained in semi-contact mode utilizing NSG01 probes from NT-MDT, featuring a typical curvature radius of 10nm, a force constant of 6N/m, and a resonant frequency of 150 kHz. All measurements were performed under ambient conditions.

The micro-Raman spectrum was taken in the backscattering configuration by Jobin Yvon T64000 spectrometer, equipped with nitrogen cooled charged coupled device detector. As an excitation source we used the 532 nm line of Ti: sapphire laser, with laser power 20 mW. The measurement was performed in the spectrum range 100 cm^{-1} to 1000 cm^{-1}.

FT-IR reflectivity measurement was carried out with a BOMMEM DA-8 FIR spectrometer. A DTGS pyroelectric detector was used to cover the wave number range from 60 to 700 cm^{-1}.

Fourier transform infrared spectroscopy (FTIR) was performed on a Thermo Scientific Nicolet iS35 spectrometer, Waltham, Massachusetts, USA. The spectra were measured in 4000 to 500 cm^{-1} range, with resolution of 4 cm^{-1}.

3. Results and discussion

X-ray analysis of 0.01 wt.% Er^{3+} doped $BaTiO_3$ samples shows only $BaTiO_3$ perovskite phase and uniform distribution of erbium. The increase of dopant content gives rise to the appearance of second phase $Er_2Ti_2O_7$ in 0.5 wt.% Er^{3+} doped $BaTiO_3$, (Fig. 2). By comparison of XRD peaks of undoped $BaTiO_3$ and Er doped $BaTiO_3$, it is evident that XRD peaks of doped samples are shifted towards to lower values of 2θ thus indicating the increase of lattice parameters, i.e. the incorporation of Er on the Ti-sites rather than on Ba-sites in $BaTiO_3$ structure.

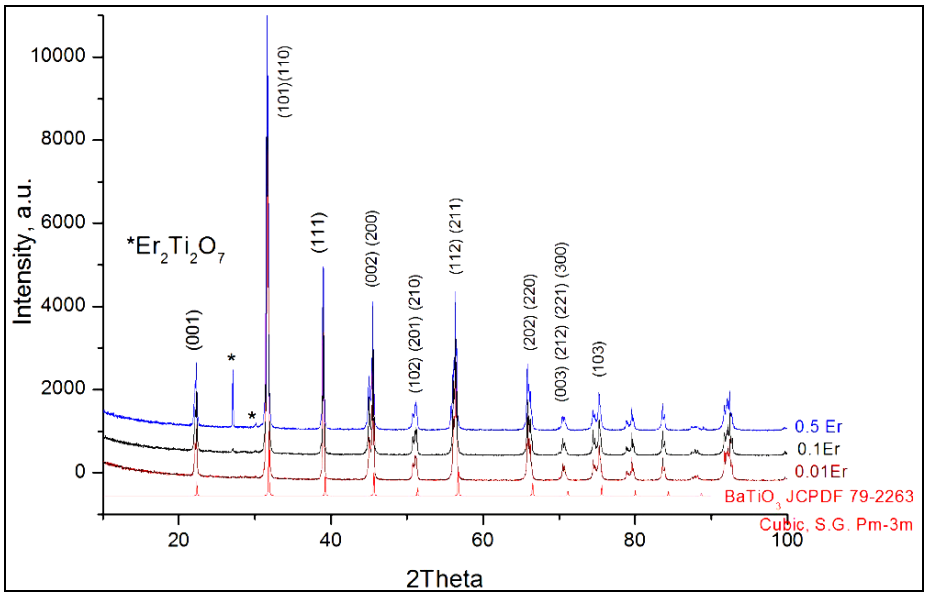

Fig. 2. X-ray diffractogram of barium titanate doped Er^{3+} (color online)

The Er_2O_3 doped $BaTiO_3$ samples are characterized by irregularly polygonal grains microstructure (Fig. 3). For samples doped with lower additive content (0.01 wt.% Er^{3+}), the abnormal growth of grains (grain size from 20 to 45 μm) for 1350 °C sintering temperature (Fig. 3a). With an increase of the additive content the average grain size decreases. As a result, for 0.5 wt.% of dopant, the average grain size is from 10 μm to 15 μm, and for the samples doped with 1.0 wt.% of dopant grain size decreased to the value of 5-10 μm (Fig. 3b).

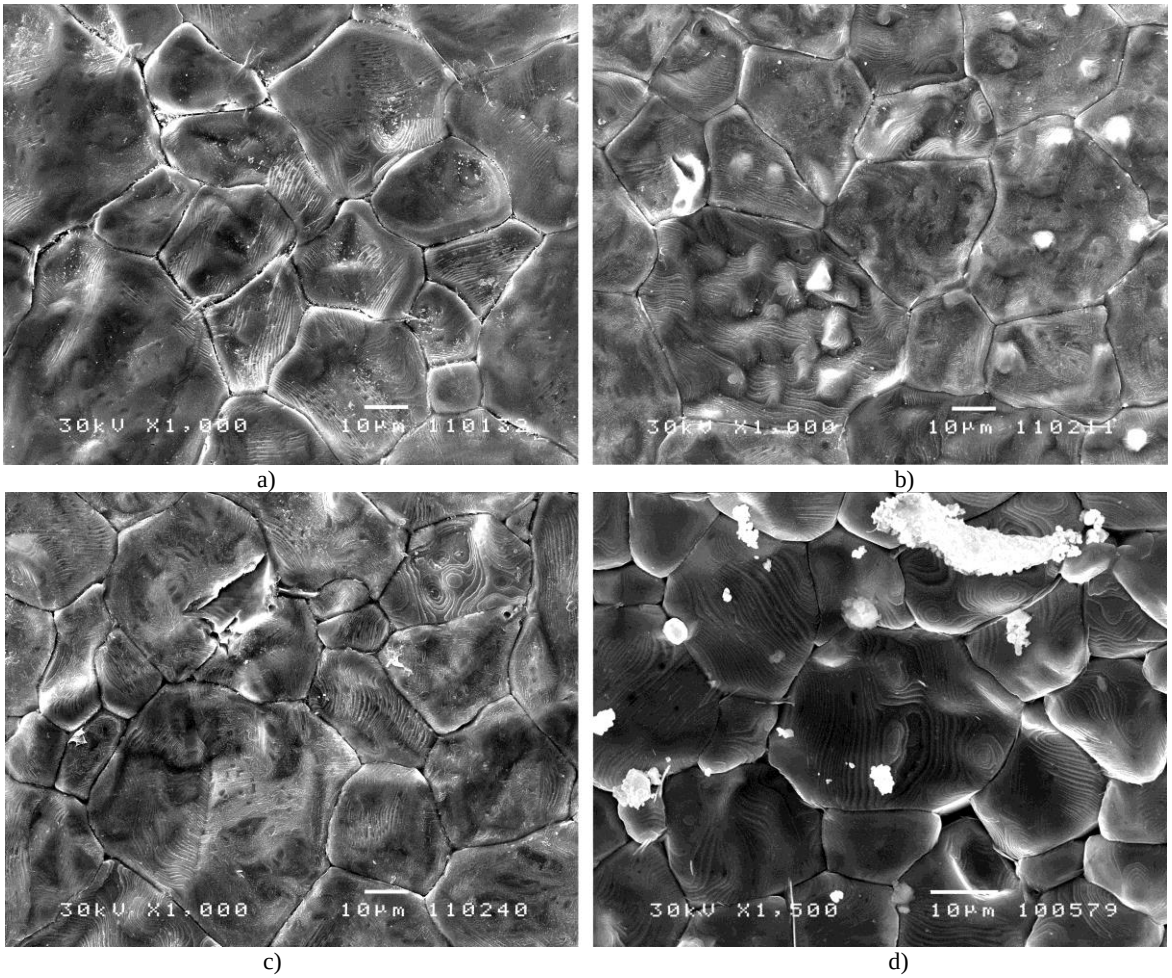

a) b)

c) d)

Fig. 3. SEM images of $BaTiO_3$ sintered at 1350 °C doped with a) 0.01, b) 0.1, c) 0.5 and d) 1.0 wt.% of Er^{3+}

EDS analysis of samples doped with 0.01 wt.% Er_2O_3 does not reveal any Er rich regions, thus indicated a uniform incorporation of dopants within the samples. It is worth noting that the concentrations less than 1.0 wt.% could not be detected by the EDS unless an inhomogeneous distribution or segregation of the additive was present. Increasing of dopant concentration leads to the appearance of Er rich regions between grains as shown in Fig. 4.

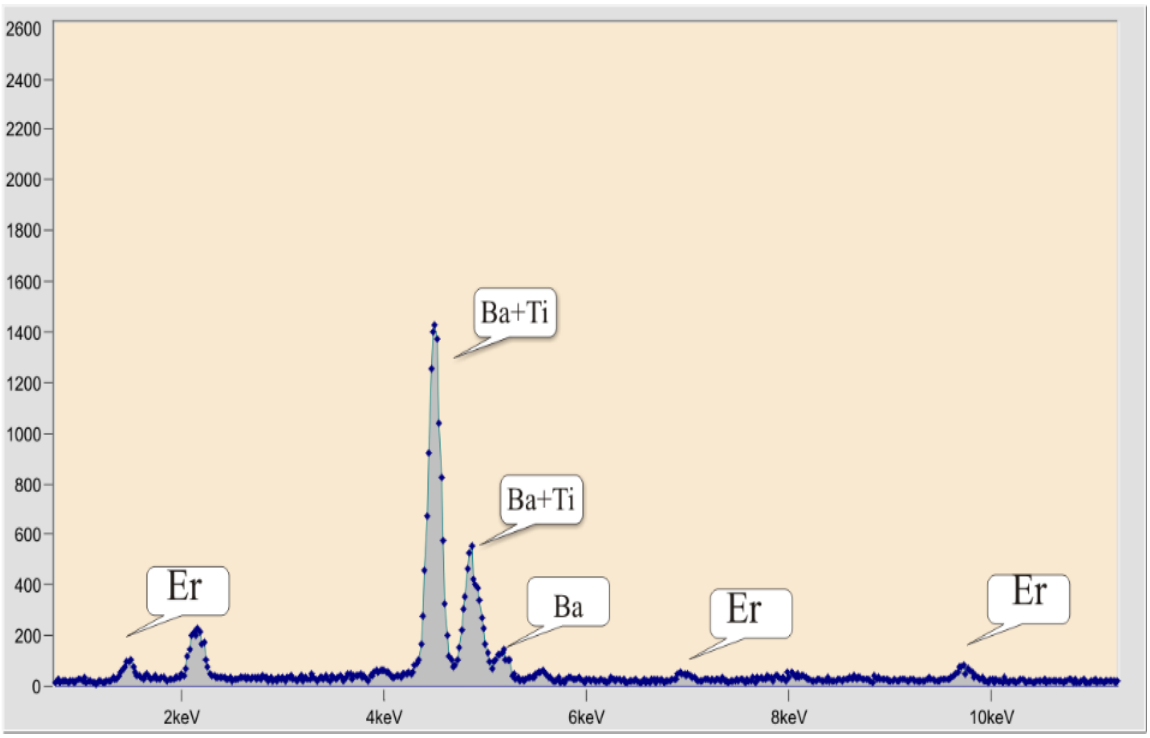

Fig. 4. SEM/EDS spectra of $BaTiO_3$ doped 1.0 wt.% Er^{3+}

The surface structure of grains, observed in SEM experiments, is investigated using AFM. The AFM analysis consists of the visual inspection of topography images of the grain surface and inspection of the corresponding root mean square (RMS) roughness. The RMS roughness is equivalent to the standard deviation of heights measured by the AFM and is consequently very sensitive to pronounced surface features such as valleys and peaks [28]. For that reason, the RMS can be used to estimate the flatness of the surface.

An example of AFM topography image recorded within a grain is shown in Fig. 5a). Visual inspection of topography images, such as the one in Fig. 5a), shows no significant differences between the grains across all concentrations of Er^{3+}. The surfaces are flat with features not exceeding 100 nm in height. This observation is corroborated by low values of the average RMS surface roughness, computed for every Er^{3+} concentration and displayed in Fig. 5b).

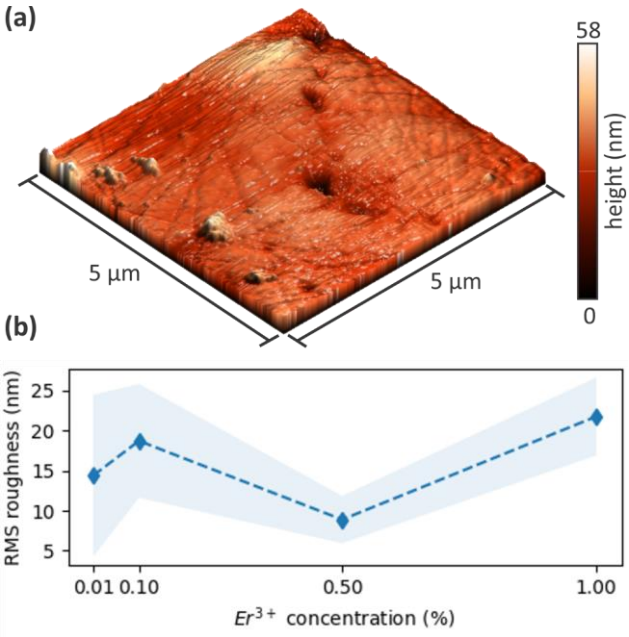

Fig. 5. a) AFM topography of a $BaTiO_3$ (0.01 wt Er^{3+}) grain. b) Average RMS roughness as a function of Er^{3+} concentration. The edges of the (blue) shaded area represent the lowest and highest RMS roughness values (color online)

Fig. 6 gives the Raman spectra of Er^{3+} doped $BaTiO_3$ at room temperature. $BaTiO_3$ is a well-known classic ferroelectric material that is cubic above 393-408 K and belongs to the space group *Pm3m* (*O1h*). At temperatures below 393 K, it is ferroelectric with a *P4mm* (*C14v*) structure, which further transforms to orthorhombic and rhombohedral structures at 278 and 183 K, respectively [29]. Optical modes of cubic phase of $BaTiO_3$ transform according to the $3F_{1u} + 1F_{2u}$ irreducible representation. The F_{1u} modes are infrared-active and the F_{1u} mode is the so called "silent mode" since it is neither infrared- nor Raman-active [30]. Each triply degenerate F_{1u} mode splits into A_1 + E phonons in the tetragonal phase whereas F_{2u} splits into an $E + B_1$ mode. These modes further split into longitudinal (*LO*) and transverse (*TO*) components because of the long-range electrostatic forces associated with lattice ionicity. The $E + B_1$ modes derived from the cubic F_{2u} mode are essentially degenerate. For other modes of tetragonal phase, the assignment of phonons as *LO* or *TO* is valid as long as the phonon wave vector lies along one of the principal symmetry directions of the crystal. For the phonons propagating in between the principal axes, mixing of the A_1 and *E* modes occurs and quasi modes appear in the spectra.

$BaTiO_3$ exhibits tetragonal structure belonging to the space group C_{4v} symmetry. All of the features observed in the tetragonal phase have been reported in the literature [31]. The peak observed at 305 cm^{-1} corresponds to the *E*(TO2) phonon mode of tetragonal $BaTiO_3$. The A_1(TO1), A_1 (TO2), A_1 (TO3) and A_1 (LO3) modes were observed at about 180, 270, 516 and 720 cm^{-1}, respectively [32]. Raman spectra obtained from Er^{3+} doped $BaTiO_3$ did not show any remarkable wavelength shift. It can also be seen that all Raman modes become weaker and broader with an increase in Er^{3+} concentration. It indicates the higher Er^{3+} concentration results in the worse crystallinity, which is consistent with the XRD results.

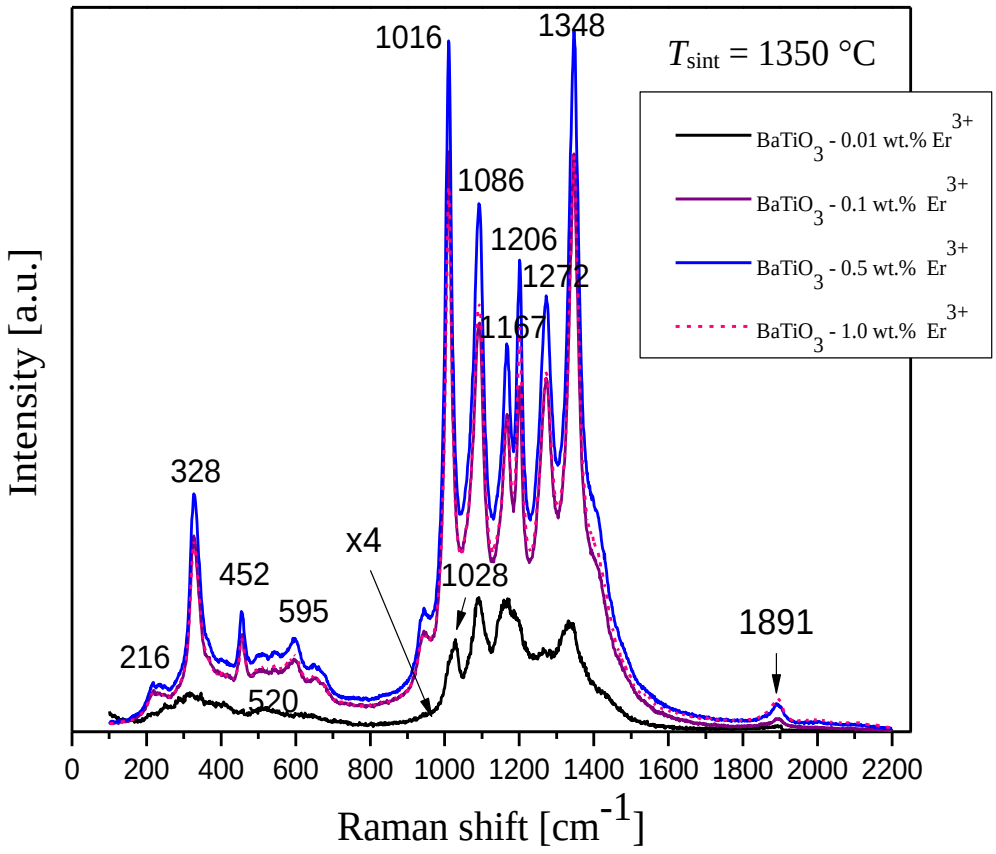

Fig. 6. Raman spectra of $BaTiO_3$ doped Er^{3+}(color online)

The Raman spectroscopy is used to analyse the structure and phase shift of doped Er^{3+} $BaTiO_3$ ceramics and examine vibrational, rotational and other low frequency modes. Fig. 6 illustrates the Raman spectra of doped $BaTiO_3$ (0.01, 0.5, 1.0 wt.% Er^{3+}) were performed from 100 to 2200 cm^{-1} at room temperature. The characteristic four different peaks (denoted by vertical lines) of tetragonal Er-BT ceramic are reported to be arising from the splitting of transverse (TO) and longitudinal (LO) photons [31]. Raman peaks were observed at about 262 cm^{-1} (A_1 (TO)), 328 cm^{-1} (B_1, *E* (TO + LO)), 512 cm^{-1} (A_1 (TO), *E* (TO)) and 719 cm^{-1} (A_1 (LO), *E* (LO)) respectively. The detected bands were matched with $BaTiO_3$-based ceramics by Ref. [31]. The peaks denoted by A_1, B_1, and *E* (TO + LO), TO_2, LO_2 vibrational modes respectively and reveal the tetragonal symmetry (*P4mm*) of $BaTiO_3$ ferromagnetic state [32] shows similar results to other researchers [30, 33]. When there is sufficient dopant content in BT so that it crosses over the point of phase transition from tetragonal to cubic,

the tetragonal phase (*P4mm*) of Raman active modes remains inactive in the perfect cubic phase (*Pm3m*) following the forbidden Raman selection rules. Besides, an intense band of 512 cm^{-1} sustained at the tetragonal phase above T_c. With the increase in Er^{3+} content the band turn into narrow and keen also a vivid change at low frequencies was observed. No significant shift in wavelength was noticed in the spectra of Er-BT but became steeper with an increase in erbium concentration which indicate enhanced crystallinity for higher Er^{3+} concent that also demonstrate similar consequence with the XRD analysis.

The Raman spectra showed an octet feature consisting of six main peaks at 367, 447, 523, 555, 628 and 703 cm^{-1} and two shoulder peaks at 303 and 787 cm^{-1}. These spectra are called the abnormal Raman spectra. Accordingly, it was inferred that a small number of Er^{3+} ions in doped samples inevitably entered Ba sites because of the amphoteric behavior of Er^{3+}, which resulted in appearance of several additional bands at 367, 447, 555, 628, 703, and 787 cm^{-1} (Fig. 6).

The IR reflectivity spectra of ceramics of $BaTiO_3$ doped Er^{3+} prepared by conventional solid-state sintering procedure is shown in Fig. 7. The bands in the lower wave number range (100-600 cm^{-1}) are due to Ti-O vibrations [34]. The Ti-O vibration is characterized by a transversal optical mode indicated at ≈ 470 cm^{-1} attributed to the stretching mode of TiO_6 octahedron. A broad band at about 540 cm^{-1}, which is typical of the Ti-O vibrations in the $BaTiO_3$ compound, starts to be developed. In the case of the doped $BaTiO_3$ ceramic there are two extra peaks at about 180 cm^{-1} (TO) and 470 cm^{-1} (LO), which could be assigned to bands of the barium oxide titanium oxide system (Fig. 8). The presence of the vibration mode ≈ 180 cm^{-1} characterizes the lattice deformation. This suggests a change of crystal structure to pseudo cubic that is in agreement with XRD observation.

The bands in the lower wave number range (100-600 cm^{-1}) are due to Ti-O vibrations [34]. The Ti-O vibration is characterized by a transversal optical mode indicated at ≈ 470 cm^{-1} attributed to the stretching mode of TiO_6 octahedron. A broad band at about 540 cm^{-1}, which is typical of the Ti-O vibrations in the $BaTiO_3$ compound, starts to be developed. In the case of the doped $BaTiO_3$ ceramic there are two extra peaks at about 180 cm^{-1} (TO) and 470 cm^{-1} (LO), which could be assigned to bands of the barium oxide titanium oxide system (Fig. 8). The presence of the vibration mode ≈ 180 cm^{-1} characterizes the lattice deformation. This suggests a change of crystal structure to pseudo cubic that is in agreement with XRD observation.

FTIR spectra of $BaTiO_3$ doped Er^{3+} samples annealed at 1350 °C are presented in Fig. 8. Shoulder band appeared in all the samples in the region 1100-900 cm^{-1}, indicating the presence of Ba and Ti oxides [1]. All of the spectra showed a broad band around 600 cm^{-1}, originating from Ti-O stretching vibrations in TiO_6 octahedron [35]. Band around 440 cm^{-1} originated from Ti-O bending vibration [36]. Presence of both bands in all samples revealed tetragonal phase of $BaTiO_3$ doped Er^{3+}.

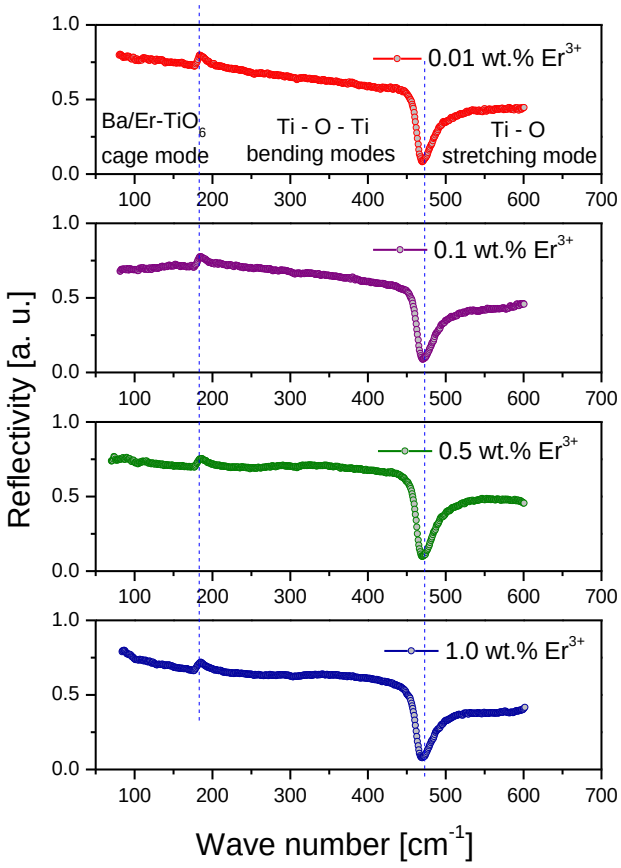

Fig. 7. IR reflectivity spectra of $BaTiO_3$ doped Er^{3+} (color online)

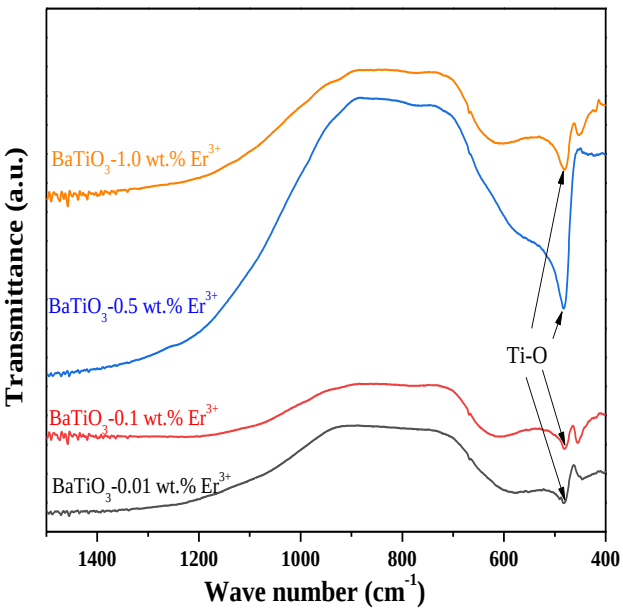

Fig. 8. FTIR spectra of $BaTiO_3$ doped Er^{3+}(color online)

However, differences in peak position indicate lattice distortion with the incorporation of Er [37]. In sample $BaTiO_3$-0.01 wt.% Er^{+3} Ti-O stretching is positioned at 593.7 cm^{-1}, while in $BaTiO_3$-0.1 wt.% Er^{3+}, $BaTiO_3$-0.5

wt.% Er^{3+} and $BaTiO_3$-1.0 wt.% Er^{3+}, it was shifted to 609.8 cm^{-1}, 572.0 cm^{-1} and 609.8 cm^{-1}, respectively. These shifts confirmed the incorporation of Er^{3+} in $BaTiO_3$ at 1350 °C.

4. Conclusion

$BaTiO_3$ doped Er^{3+} ceramics have been successfully obtained through the conventional solid-state reaction route. The ceramics sintered at 1350 °C. The microstructure and the optical properties were investigated. The structural evolution of solid solutions was monitored by X-ray diffraction, scanning electron microscopy, Raman and FTIR spectroscopy. A double deflexion located at $2\theta \approx 46°$ showed the formation of the tetragonal ferro-electric phase for the patterns in which Er^{3+} content was $0.001 \leq x \leq 1.0$. A secondary phase belonging to *Fd3m* space group identified as a pyrochlore ($Er_2Ti_2O_7$) was revealed at the position $2\theta \approx 28°$, $2\theta \approx 29.6°$ and $2\theta \approx 35.36°$. The solubility limit of Er^{3+} in the crystal structure of $BaTiO_3$ was reached when $x = 0.05$. The SEM micrographs consisted of rounded grains with a wide grain-size distribution. The EDS analysis confirmed the presence of the Er^{3+} in the crystalline structure of $BaTiO_3$. The Raman graphics showed the typical $BaTiO_3$ tetragonal phase scattering bands at around 250, 520 and 720 cm^{-1}, and a sharp peak at around 306 cm^{-1}. An extra band was observed about 1834 cm^{-1}, when Er^{3+} content was Er $0.10 \leq x \leq 1.0$. This result can be associated to the formation of the secondary phase ($Er_2Ti_2O_7$) identified by X-ray diffraction. The Infrared spectroscopy patterns indicated the characteristic bands relating to $BaTiO_3$.

Acknowledgment

The authors acknowledge funding provided by the Institute of Physics Belgrade, the Vinča Institute of Nuclear Sciences (Contract No. 451-03-66/2024-03/200017), University of Belgrade, and Faculty of Electronic Engineering, University of Niš (Grant No. 451-03-65/2024-03/200102) through the financial support of the Ministry of Science, Technological Development, and Innovation of the Republic of Serbia. This research was supported by the Science Fund of the Republic of Serbia, Grant No. 7504386, Nano object in own matrix – Self composite – NOOM-SeC.

References

[1] A. Meneses-Franco, M. Campos-Vallette, S. Octavio Vásquez, E. A. Soto-Bustamante, Materials **11**, 1950 (2018).
[2] C. Pithan, D. Hennings, R. Waser, Int. J. Appl. Ceram. Tech. **2**(1), 1 (2005).
[3] D. H. Kuo, C. H. Wang, W. P. Tsai, Ceramics International **32**, 1 (2006).
[4] V. Paunović, V. V. Mitić, M. Đorđević, M. Marjanović, L. Kocić, Sci. Sintering **49**, 129 (2017).
[5] H. X. Z.hang, C. H. Kam, Y. Zhou, X. Q. Han, S. Buddhudu, Y. L. Lam, Opt. Mater. **15**, 4750 (2000).
[6] G. Schlaghecken, J. Gottmann, E. W. Kreutz, R. Poprawe, Appl. Phys. A **79**, 1255 (2004).
[7] Y. Umeda, K. Masuzawa, S. Ueda, S. Ootsuki, A. Kuwabara, H. Moriwake, Ceram. Int. **38**, S25 (2012).
[8] W. Strek, D. Hreniak, G. Boulon, Y. Guyot, R. Pązik, Opt. Mater. **24**, 15 (2003).
[9] A. García Murillo, F. J. Carrillo Romo, M. García Hernández, O. Barbosa García, A. Meneses Nava, S. Palomares Sánchez, A. Flores Vela, Mater. Trans. **50**, 1850 (2009).
[10] M. García-Hernández1, A. García-Murillo, F. de J. Carrillo-Romo, Á. de J. Morales-Ramírez, M. A. Meneses-Nava, B. Gonzalez-Penguelly, V. Garibay Febles, Mater. Trans. **54**(5), 806 (2013).
[11] S. Wang, G. O. Dayton, J. Am. Ceram. Soc. **82**(10), 2677 (1999).
[12] M. Wegmann, R. Bronnimann, F. Clemens, T. Graule, Sens. Actuators A: Phys. **135**(2), 394 (2007).
[13] P. Kumar, S. Singh, J. K. Juneja, C. Prakash, K. K. Raina, Ceramics International **37**, 1697 (2011).
[14] Z. C. Li, B. Bergman, J. Eur. Ceram. Soc. **25**, 441 (2005).
[15] V. Mitic, V. Paunovic, D. Mancic, Lj. Kocic, Lj. Zivkovic, V. B. Pavlovic, Ceramic Transactions **204**, 137 (2009).
[16] N. H. Chan, D. M.Smyth, J. Am. Ceram. Soc. **67**(4), 285 (1984).
[17] V. Paunovic, Lj. Zivkovic, V. Mitic, Sci. Sintering, **42**(1), 69 (2010).
[18] R. Zhang, J. F. Li, D. Viehland, J. Am. Ceram. Soc. **87**(5), 864 (2004).
[19] P. W. Rehrig, S. Park, S. Trolier-McKinstry, G. L. Messing, B. Jones, T. Shrout, J. Appl. Phys. **86**(3), 1657 (1999).
[20] V. Mitić, Z. Nikolić, V. Pavlović, V. Paunović, M. Miljković, B. Jordović, Lj. Zivković, J. Am. Ceram. Soc. **93**(1), 132 (2010).
[21] E. J. Lee, J. Jeong, Y. H. Han, Jpn. J. Appl. Phys. **45**, 822 (2006).
[22] S. M. Park, Y. H. Han, J. Korean Phys. Soc. **57**(3), 458 (2010).
[23] K. J. Park, C. H. Kim,Y. J. Yoon, S. M. Song, J. Eur. Ceram. Soc. **29**, 1735 (2009).
[24] V. Paunovic, V. Mitic, M. Marjanovic, Lj. Kocic, Facta Universitatis, Series: Electronics and Energetics **29**(2), 285 (2016).
[25] S. Islam, N. Khatun, Md. S. Habib, S. F. Uddin Farhad, N. I. Tanvir, Md. A. Ali Shaikh, S. Tabassum, D. Islam, Md. Sajjad Hossain, A. Siddika, Heliyon **8**, e10529 (2022).
[26] M. T. Buscaglia, M. Viviani, V. Buscaglia, C. Bottino, P. Nanni, J. Am. Ceram. Soc. **85**(7), 1569 (2002).
[27] J. Qi, Z. Gui, Y. Wang, Q. Zhu, Y. Wu, L. Li,

Ceramics International **28**, 141 (2002).
[28] Z. V. Ooi, A. A. Saif, P. Poopalan, Malaysian Journal of Microscopy **11**, 89 (2015).
[29] B. Jaffe, W. Cook, H. Jaffe, Piezoelectric Ceramics, Academic Press: London, 1971.
[30] R. Loudon, Adv. Phys. **13**(52), 423 (1964).
[31] P. S. Dobal, R. S. Katiyar, J. Raman Spectrosc. **33**(6), 405 (2002).
[32] Y. Zhang, J. Hao, C. Leung Mak, X. Wei, Optics Express **19**(3), 1824 (2011).
[33] Lu Da-Yong, Wei Cheng, Sun Xiu-Yun, Liu Qiao-Li, Li De-Xu, Li Zhong-Yu, J. Raman Spectrosc. **45**, 963 (2014).
[34] R. Ashiri, Vibrational Spectroscopy **66**, 24 (2013).
[35] Thi Tuyet Mai Phan, Ngoc Chau Chu, Van Boi Luu, Hoan Nguyen Xuan, Duc Thang Pham, Isabelle Martin, Pascal Carrière, J. Sci.: Adv. Mater. Dev. **1**, 90 (2016).
[36] T. Xian, H. Yang, L. Di, J. Ma, H. Zhang, J. Dai, Nanoscale Research Letters **9**, 327 (2014).
[37] M. Tihtih, J. E. F. M. Ibrahim, M. A. Basyooni, R. En-nadir, I. Hussainova, I. Kocserha, ACS Omega **8**, 8448 (2023).

*Corresponding author: lzorica@yahoo.com